PROCEEDINGS OF PAPERS

Zbornik radova

(Ic)ETRAN 2019

6th International Conference on Electrical, Electronic and Computing Engineering

in conjunction with

ETRAN

63rd National Conference on Electrical, Electronic and Computing Engineering

Proceedings of Papers – 6th International Conference on Electrical, Electronic and Computing Engineering, IcETRAN 2019, Silver Lake, Serbia, June 03 – 06, 2019

Zbornik radova - 63. Konferencija za elektroniku, telekomunikacije, računarstvo, automatiku i nuklearnu tehniku, Srebrno jezero, 03 – 06. juna, 2019. godine

Main Editor / Glavni urednik
Dejan Popović

Editors / Urednici
Slobodan Vukosavić, Boris Lončar

Published by / **ETRAN Society, Belgrade, Academic Mind, Belgrade**
Izdavači / **Društvo za ETRAN, Beograd i Akademska misao, Beograd**

Production / Izrada
Academic Mind, Belgrade / Akademska misao, Beograd

Place and year of publication / Mesto i godina izdanja
Belgrade, 2019. / Beograd, 2019.

Circulation / Tiraž
200 primeraka / 200 copies

ISBN 978-86-7466-785-9

www.etran.rs

Influence of Mechanical Activation on Electrical Properties of Ceramic Materials in VHF Band

Nina Obradović and Antonije Đorđević

***Abstract*—Mechanical activation is commonly used as a pre-sintering process in order to enhance the reactivity of materials, reduce the particle size, increase diffusion rates, accelerate the reaction, and lower the sintering temperature. The mechanical activation can affect the final electrical and mechanical characteristics. In this paper we consider the influence of the mechanical activation on the permittivity and the loss tangent. We outline methods for evaluation of these parameters, with emphasis on our coaxial-chamber technique for measurements in the VHF band.**

***Index Terms*—Ceramic materials; mechanical activation; sintering; electrical properties; numerical modeling; measurements of dielectric parameters.**

I. Introduction

Ceramic materials are solid materials obtained by sintering of appropriate mixtures of powders. "Ceramic" is derived from the Greek word "keramos", which means potter's clay or pottery [1]. Ceramic materials have many technical applications. Advanced materials, such as alumina, aluminum nitride, borides, zirconia, silicon carbide, silicon nitride, silicon- and titania-based materials offer a high-performance and economic alternative to conventional materials, such as glass, metals, and plastics.

The sintering is one of the most important phases in the production process of ceramic materials. Specific predetermined properties of ceramics are required along with cost-effectiveness of the manufacturing process [2]. In order to obtain materials with the desired properties during the sintering process, one should simultaneously take into account several factors: the size, shape, and structure of the particles, particle-size distribution, particle packing, the purity of the starting mixtures, the density of compacts (samples obtained after consolidation, prior to the sintering process), the appropriate sintering regime (temperature and sintering time, heating/cooling rate), the atmosphere in which the process is performed, the existence of impurities and/or additives, etc. It has been empirically determined that a decrease in the particle size of reactants leads to an increase of the isothermal process constant rate without changes in the activation energy of the process [3]. The increase of the specific surface area that is induced by the mechanical activation plays an important role. Extremely small particles require application of a higher pressure during the consolidation process. Due to the non-homogeneous package and gas retention, samples get stratified and the sintering leads to formation of cracks. The presence of large particles causes an excessive grain growth during the sintering. By adjusting the conditions of the pre-treatment, we can prepare the starting powder with the predefined optimal particle-size distribution.

Basically, the sintering processes can be divided into two types: the solid-state sintering and the liquid-phase sintering. The solid-state sintering occurs when the powder compact is densified wholly in the solid state at the sintering temperature. The liquid-phase sintering occurs when a liquid phase is present in the powder compact during the sintering [4].

Ceramic materials are used in electrical engineering as insulators, chip carriers, dielectrics for capacitors, in fabrication of multilayer ceramic (MLC) devices, in particular LTCC (low-temperature co-fired ceramics), for various optical devices, etc. Various properties of these materials are important, depending on the application. The relevant electromagnetic properties of the sintered materials include dielectric properties (permittivity, losses, and breakdown), insulating/conductive properties, magnetic properties (permeability, losses, nonlinearities, and Curie temperature), and possible piezoelectric properties. The thermal conductivity is important for heat transfer in semiconductor devices. Adherence of metals and semiconductors, including dilatation and compatibility with adhered materials, is essential for fabrication processes, etc.

In this paper, we consider only nonmagnetic materials and are focused on the electrical properties of the ceramics. We assume that the material is linear. We consider the complex relative permittivity and quantities related to it (the loss tangent and the conductivity), predominantly in the VHF (Very High Frequency) band, which extends from 30 MHz to 300 MHz. Fig. 1 presents the position of the VHF band in the spectrum. The data include free-space wavelength (λ), the frequency (f), the energy of a quantum, and the designation.

We present our measurement technique for the relative permittivity of ceramic samples in the VHF band, which can also be applied in higher frequency bands, in the microwave region, up to around 10 GHz.

This paper is organized as follows. In Section II, we briefly present methods of mechanical activation and the sintering process. In Section III, the complex permittivity is introduced. In Section IV, we provide a description of our measurement technique. In section V, we give examples of measured permittivities of ceramic materials. Finally, Section VI concludes the paper.

Nina Obradović – Institute of Technical Sciences of SASA, Knez Mihailova 35/IV, 11000 Belgrade, Serbia (e-mail: nina.obradovic@itn.sanu.ac.rs).

Antonije Đorđević – School of Electrical Engineering, University of Belgrade, Bulevar kralja Aleksandra 73, 11120 Belgrade, Serbia, and Serbian Academy of Sciences and Arts, Knez Mihailova 35, 11000 Belgrade, Serbia (e-mail: edjordja@etf.bg.ac.rs).

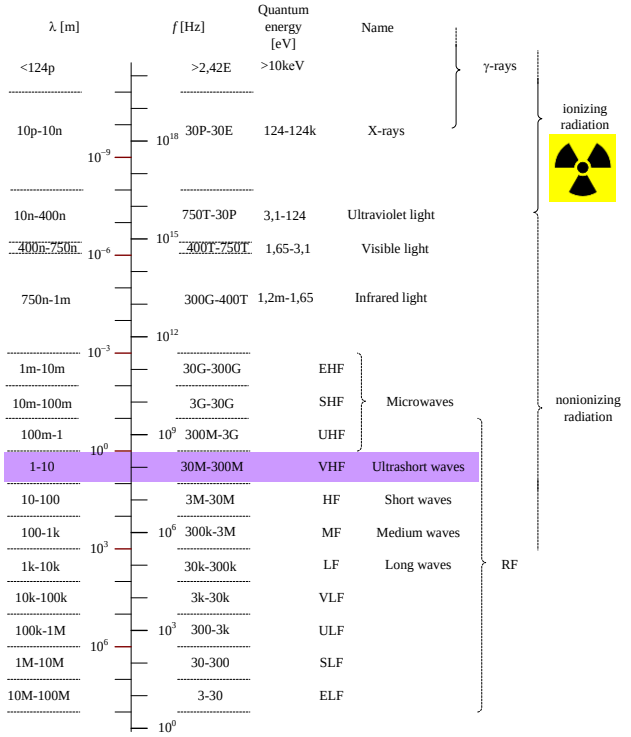

Fig. 1. Position of the VHF band in the electromagnetic spectrum.

II. Mechanical Activation and Sintering

The mechanical activation represents a complex physico-chemical process, which leads to an increase of chemical activity and potential energy of the treated material. Such a process can cause changes in the specific surface area and internal energy within the system. The free energy of the system is also increased [5]. During the mechanical activation of an inorganic material, attrition of the material takes place and reduces the crystallite size, which further leads to deformation or changes in the crystal structure, accompanied by generation of defects [6–9]. Grinding of the material is carried out by successive fracturing of particles (Fig. 2). The method of obtaining the finest powder is called dispersion milling [10]. Equipment used for grinding is a mill. There are several types of high-energy mills: attrition mill, vibro mill, horizontal ball mill, and planetary mill.

In terms of the grinding process, the influence of the mechanical forces on the material leads to formation of elastic and plastic deformations. During the elastic collision, the whole energy of the system remains unchained, as well as the material structure. During the plastic collision, the energy is partially transformed into the energy of deformation. Physico-chemical properties of materials are changed by these deformations [11]. The reaction capability of solid materials increases as a direct result of structural changes within the material by applying the method of mechanical activation. Changes of the structure of the crystal lattice are reflected trough the generation of point defects (vacancies, interstitial atoms, and impurity atoms), line defects (atom aggregations on the crystal surface), volume defects (pores and impurities), and electron defects (electrons and holes) [12, 13]. The occurrence of defects during mechanical activation represents the general tendency of crystals to transform the mechanical energy into the energy of the crystal lattice defects. During the mechanical treatment, the condition of the treated system is constantly changing, from the stage of the initial powder, where particles are poorly connected, to the stage of a heterogeneous system, where larger agglomerates form out of smaller powder particles with clearly defined boundaries.

Grinding of the material is carried out by successive fracturing of the powder particles in the mills. The mechanical activation leads to fragmentation, decrease of the particle size, and change of the free surface and the physico-chemical properties of crushed material. It is performed in order to improve the reactivity of the system or for the purpose of its amorphization. This treatment increases the reactivity of the material and lowers the temperature and time of sintering [15, 16].

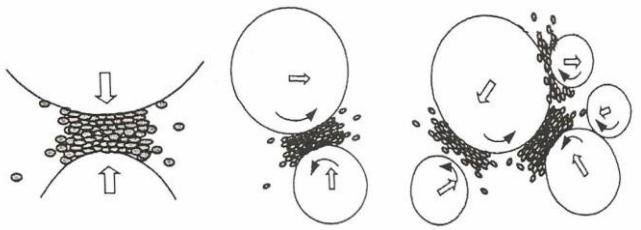

Fig. 2. Collisions that occur during milling in a high-energy planetary ball mill [14].

The method of mechanical activation has a variety of advantages compared to other methods of powder preparation, such as relatively cheap equipment (mills), inexpensive production, possible appliance to all classes of materials, and obtaining large quantities of material for further investigation. The main disadvantage of this method is the formation of agglomerates in the powder after milling. The powder agglomeration can be controlled and avoided by choosing adequate synthesis parameters. Firstly, the time of activation. According to the literature data, authors apply times in the range of two to five minutes, adequate for mixing and homogenization of powders [17, 18], up to dozens of hours, in cases of very hard materials or difficult and complex reactions occurring in the system [19–21]. Secondly, the ball-to-powder mass ratio. Authors choose the ball-to-powder mass ratio depending on how much energy they wish system to get during milling. Authors usually choose 20:1 or 40:1 ball-to-powder mass ratio, in order to obtain great energy transfer and easier and faster mechanochemical reaction [22–24]. Thirdly, selection of the material that the mill is made of. There is a variety of materials in usage, such as ZrO_2, WC-Co or hardened steel [25–27]. There is a possibility that during prolonged activation some particles from balls and vessels drop off and incorporate into the powder particles. Hence, prolonged milling time is not very suitable or milling equipment needs to be new and unused. Finally, the choice of the milling medium is also very important. It could be dry milling, conducted in air, or wet milling, e.g., in ethanol [28, 29]. Usually, milling is performed in air, but if the objective is to avoid the agglomerates, wet milling can be performed. To protect the powders from oxidation, the milling can take place in an inert atmosphere (at atmospheric pressure), either Ar or N_2 [30]. The method of mechanical activation attracts great attention due to its simplicity and because many parameters can be changed and optimized, which makes the work in a laboratory interesting, challenging, and novel each time.

G. V. Samsonov gave the most complete definition of the sintering process: “Sintering is a set of complex and interconnected mass transport processes that occur between the particles and within the particles of dispersed system during its consolidation” [31]. The necessary energy needs to be transferred into the system, so the sintering process can take place. It can be thermal (heating), mechanical (sintering under high pressure), or of some other form of energy (e.g., microwave sintering). The free energy of the system, which is in the non-equilibrium state, represents a driving force for the sintering process. The non-equilibrium state is a consequence of a developed specific surface area of powder particles and structural defects within them.

The sintering process of real materials can be conditionally divided into three stages [15], as illustrated in Fig. 3:

(1) In the initial stage, a contact is made between individual particles, but particles retain their structural individuality. During this stage, the density changes slightly and at the end of this stage, its value is 60–75 % of the theoretical density. At this sintering stage, the establishment of a better contact between particles and neck growth are a consequence of simultaneous acting of several mechanisms (viscous flow, surface diffusion, and volume diffusion). Open porosity is dominant, with pores of irregular shape and fracture trough grains.

(2) In the middle stage, particles accrue to one another. This leads to fast growth of contact necks, space between particles loses its shape, and particles lose their individuality. Pores get a more regular shape; their closure begins along with grain growth. Densification is most intensive in this intermediate phase. Fractures between grains and fractures trough grains are present at this sintering stage.

(3) The final stage is characterized by further formation of closed pores and grain growth. Due to shrinkage, open pores are too narrow to be stable and they are transformed into closed pores; then sintering enters the final stage. Density values are 90–93 % of the theoretical density. The final sintering stage is characterized by elimination of closed pores and approaching the theoretical density. The volume diffusion and diffusion along grain boundaries are dominant in the middle and final sintering stages. There are no sharp boundaries between these three stages of sintering.

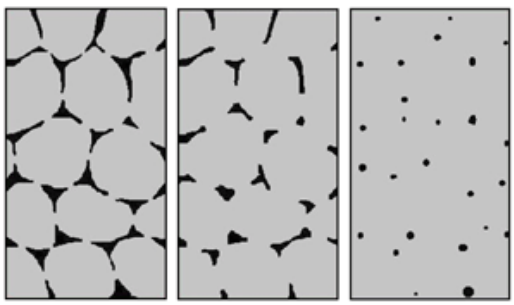

Fig. 3. The three stages of solid-state sintering [32].

In practice, technological factors have a great influence on the sintering process. Most important are: particle shape and size within the initial powder, the purity of the starting powders, the density of compacts (compaction pressure), sintering temperature, sintering regime, sintering atmosphere, etc.

There are a number of equations describing the process of sintering in the literature, which certainly indicate the great complexity of the process. Each of these equations refers to either the individual stages of sintering, or to certain mechanisms. Therefore, the basic questions concerning the kinetics and mechanisms are solved by usage of models (two-sphere model, sphere and flat plain model, etc.). A two-sphere model is most commonly used (Fig. 4). An increase of the contact surface may be caused by several mechanisms. Different types of diffusion in a solid state allow transport of the mass:

(1) The viscous flow consists of a deformation of the crystal structure under the influence of the surface tension. The mass transport occurs owing to the directional movement of atoms from the volume of the particles to the contact neck. During this process, the work that is carried out by the forces of the surface tension is equated with the work of forces of internal friction. An increase of the contact neck occurs along with reducing the distance between the particles [33].

(2) The surface diffusion is the most general mechanism which occurs during the sintering of crystalline materials. The spontaneous transport of atoms on the particle surface is dominant. During the growth of the contact neck, the distance between particle centers remains the same, without an increase in density of the material. The surface diffusion is the most common mechanism for lower temperatures of sintering and small particles.

(3) The volume diffusion is a mechanism where the mass transfer occurs by the diffusion flow from the particle surface to the contact neck. During this type of sintering, the vacancy concentration has a great impact on the diffusion velocity. This is crucial for materials with additives, where vacancies depend directly on the concentration of dopants. In this way, the concentration of the added material has an impact on the diffusion coefficient, and consequently on the mass transfer.

(4) The evaporation-condensation is a mechanism where the mass transfer occurs due to the difference of the vapor pressure of the solid phase in various parts of the system. Owing to the existence of a higher vapor pressure of the solid phase on the convex surface, and a lower vapor pressure of the solid phase on the concave surface, the material evaporates from the convex surface and via the gas phase gets transferred to the concave surface, where it condenses. The distance between the particles does not change; hence, the evaporation-condensation mechanism does not contribute to the densification of the system.

(5) The diffusion along grain boundaries is a mechanism in which the mass transport occurs from the border area between the particles to the surface of the contact neck, by diffusion along the edge. The contribution of this mechanism to the total mass transport is not large because the extent of the grain boundaries is limited. The diffusion of substances from the grain border area to the surface of the contact neck ensures particle approaching, and produces the effect of a compact shrinkage during sintering. It also causes a change in the shape and size of pores, reducing the porosity.

One of the most important issues that need to be understood in the context of studying the process of

sintering is the way of pore elimination.

Based on experimental data, it was concluded that materials which contain large pores are sintered slower, while the smaller pores can be eliminated from the system during heating at significantly lower temperatures. The system will enter the final sintering stage when the temperature is sufficient to ensure an increase in the grain size by that level where the critical pore size reaches the size of the largest pore in the system. When the system reaches the phase where all pores are smaller than the critical pore size, it may result in a full densification of the ceramic material. That explains the poor sinterability of agglomerated powders [34].

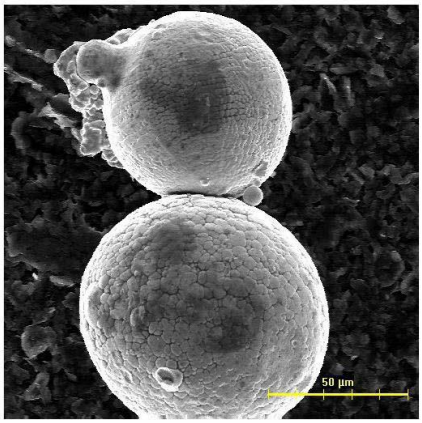

Fig. 4. An accretion of two real particles obtained by scanning electron microscopy [14].

Agglomerates are sets of small related particles that form large pores in the compact during the sintering process. As the process progresses, pores between agglomerates become larger, while pores within the agglomerates are reduced. The agglomeration or other processes, whose action makes a different pore size, suppress the sintering as long as there are two types of pores in the structure—larger ones between the agglomerates and smaller ones within the agglomerates. As the process develops, the large pores grow, while the smaller ones decrease. In the case of samples with a high initial density (the density after the compaction process, prior to the sintering), the pores between the agglomerates are reduced, and the negative effect of the existence of the two types of pores is decreased [35, 36].

Various techniques have been developed to obtain dense ceramics with a desired microstructure and phase composition. In general, these methods involve a combination of a heating regime and applied pressure. Heating regimes can be simple, as in the isothermal sintering, or can have a complex temperature-time relationship, as in the rate-controlled sintering, while the pressure may be applied either uniaxally, with or without a die, or by a surrounding gas [37]. The control of the sintering atmosphere is also important, and a precise control of oxygen or nitrogen partial pressures as a function of temperature may in some cases be beneficial or essential. Insoluble gas trapped in closed pores may obstruct the final stages of densification; hence, a change in the sintering atmosphere or a vacuum sintering is required. There are various heating regimes, such as: isothermal sintering, constant-heating-rate sintering, multi-stage sintering, rate-controlled sintering, microwave sintering, spark-plasma sintering, hot pressing, and hot-isostatic pressing.

Before we can chose the appropriate pre-sintering treatment and adjust its parameters, it is very important to have in mind that the resulting structure of the obtained compound is a direct result of structural changes at all hierarchical levels, caused by the applied treatment. It is possible to influence the development of the microstructure and to achieve the optimum and desired properties of the final material by a proper choice of the pre-sintering treatment and the type of the sintering process.

III. Complex Permittivity

In this paper, we consider dielectric properties of ceramic materials. These properties can be described by various parameters, such as polarizability, permittivity, dissipation factor (loss tangent), etc. In engineering applications, the complex relative permittivity is often used to characterize a dielectric material.

From the engineering standpoint, we live in the time domain: various physical quantities are functions of time, such as voltages, currents, electric fields, etc. In reality, the time dependence is known only for the past. However, in order to enable a mathematical description, we often assume that the time dependence is given analytically, by a certain mathematical function.

Furthermore, our world is causal: the response to a given excitation cannot occur before the excitation starts. If we consider electromagnetic waves, we even have a delay due to the propagation, so that the response is delayed after the excitation. The fastest known propagation is in a vacuum, where the velocity is $c_0 = 2{,}99792458 \cdot 10^8$ m/s .

In the engineering analysis, time-harmonic (sinusoidal) functions are often used to describe various periodic physical quantities [38]. Such functions also occur in the Fourier analysis. For example, a time-harmonic current, shown in Fig. 5, is given in the standard (canonical) form as

$$i(t) = I_\mathrm{m} \cos(\omega t + \psi), \qquad (1)$$

where t is the time ($-\infty < t < +\infty$), I_m is the amplitude ($I_\mathrm{m} \geq 0$), $\omega = 2\pi f$ is the angular frequency and f is the frequency, whereas ψ is the initial phase (usually reduced to the interval $-\pi < \psi \leq \pi$). The period (T) and the frequency are related as $fT = 1$.

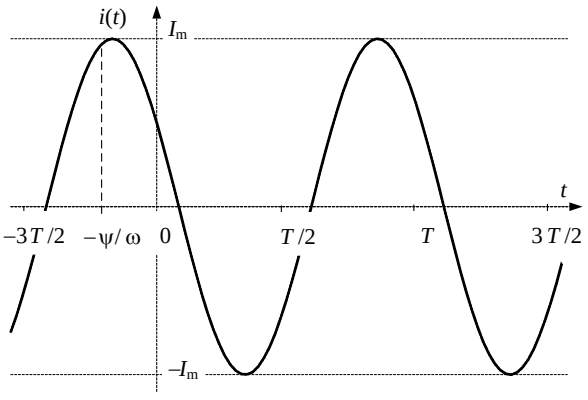

Fig. 5. Time-harmonic current.

Time-harmonic functions cannot occur in reality, because they span infinite time ($-\infty < t < +\infty$), but they can

conveniently describe various quantities in electrical engineering. In particular, if we consider a linear system and apply a time-harmonic excitation, the response will, in most practical cases, also be a time-harmonic function.

However, there are several difficulties in the analysis of such systems. The main one occurs when evaluating a sum or a difference of two time-harmonic quantities. The result is also a time-harmonic quantity of the same frequency, but expressions for the amplitude and phase of the result are rather cumbersome.

This difficulty is bypassed by introducing phasor (complex) representatives of the time-domain quantities and performing the analysis in the frequency (complex) domain. For example, the complex representative $\underline{I}$ of the time-domain current (1) is introduced by:

$$i(t) = \mathrm{Re}\left\{ \underline{I}\sqrt{2}\, \mathrm{e}^{-\mathrm{j}\omega t} \right\}, \tag{2}$$

where Re denotes the real part, $\mathrm{e} = 2.718281\ldots$ is the base of the natural logarithm, and $\mathrm{j} = \sqrt{-1}$ is the imaginary unit. In the exponential form, $\underline{I} = I\mathrm{e}^{\mathrm{j}\psi}$. The modulus (magnitude) of $\underline{I}$ is the root-mean-square (rms) value of $i(t)$, $I = |\underline{I}| = \frac{I_\mathrm{m}}{\sqrt{2}}$, and the argument (angle) of $\underline{I}$ is the initial phase of $i(t)$. Note that (2) is related to the Fourier and Laplace transforms.

Once we have phasors, addition and subtraction in the time domain is replaced by addition and subtraction of phasors, which is easily performed because we merely have to add or subtract complex numbers.

Additionally, the phasors facilitate solutions of linear differential equations: the differentiation in the time domain is mapped into the phasor domain as a multiplication by $\mathrm{j}\omega$. Hence, a linear differential equation in the time domain is mapped into an algebraic equation in the complex domain.

Equation (2) is valid for scalar quantities. A similar mapping can be applied to time-harmonic vectors as well [39]. Let us first define a time-harmonic vector, e.g., the electric-field vector, $\mathbf{E}(t)$. In Cartesian coordinates,

$$\mathbf{E}(t) = \mathbf{u}_x E_x(t) + \mathbf{u}_y E_y(t) + \mathbf{u}_z E_z(t), \tag{3}$$

where $\mathbf{u}_x$, $\mathbf{u}_y$, and $\mathbf{u}_z$ are the unit vectors of the Cartesian system, and

$$E_x(t) = E_x\sqrt{2}\cos(\omega t + \theta_x), \tag{4}$$

$$E_y(t) = E_y\sqrt{2}\cos(\omega t + \theta_y), \tag{5}$$

$$E_z(t) = E_z\sqrt{2}\cos(\omega t + \theta_z) \tag{6}$$

are time-harmonic functions of the same angular frequency ω, but can have different rms values (E_x, E_y, E_z) and initial phases ($\theta_x, \theta_y, \theta_z$). The complex representative of $\mathbf{E}(t)$ is now defined as

$$\underline{\mathbf{E}} = \mathbf{u}_x \underline{E}_x + \mathbf{u}_y \underline{E}_y + \mathbf{u}_z \underline{E}_z, \tag{7}$$

where $\underline{E}_x$, $\underline{E}_y$, $\underline{E}_z$ are the complex representatives of the components $E_x(t)$, $E_y(t)$, and $E_z(t)$, defined in accordance with (2).

Note that the complex domain is only a mathematically introduced "parallel world". Phasors (complex representatives) cannot be physically related to time-domain quantities.

The state in a polarized dielectric is macroscopically described by the polarization vector, **P** [40]. In the analysis of electromagnetic fields, in order to avoid dealing with the polarization vector, the electric displacement vector is introduced as defined by:

$$\mathbf{D} = \varepsilon_0 \mathbf{E} + \mathbf{P}, \tag{8}$$

where:

$$\varepsilon_0 = \frac{1}{\mu_0 c_0^2} = \frac{25\cdot 10^5}{299792458^2\,\pi}\ \mathrm{F/m} \tag{9}$$

is the permittivity (dielectric constant) of a vacuum. If the dielectric is linear, then the polarization vector is linearly proportional to the electric field (**E**) and, consequently, the vector **D** is also linearly proportional to **E**:

$$\mathbf{D} = \varepsilon \mathbf{E}, \tag{10}$$

where ε is the absolute permittivity (dielectric constant). Further, we can set $\varepsilon = \varepsilon_\mathrm{r}\varepsilon_0$, where ε_r is the relative permittivity (relative dielectric constant) of the material. Generally, a linear dielectric may be anisotropic (e.g., quartz), when the vectors **D** and **E** are not collinear, and ε_r is a tensor. In this paper, however, we assume the dielectric to be isotropic, so that **D** and **E** are collinear, and ε_r is a scalar. Note that $|\mathbf{D}| = |\varepsilon||\mathbf{E}|$. For a vacuum, $\varepsilon_\mathrm{r} = 1$. For static fields in linear, isotropic dielectrics, $\varepsilon_\mathrm{r} > 1$.

If the dielectric is located in a time-varying electric field $\mathbf{E}(t)$, the polarization vector is a function of time, $\mathbf{P}(t)$. Hence, the displacement vector is also a function of time, $\mathbf{D}(t) = \varepsilon_0\mathbf{E}(t) + \mathbf{P}(t)$. As a particular case, in the time-harmonic regime, all three vectors are time-harmonic quantities. However, in the general case, they are not in phase. If we switch to the complex domain, we can write

$$\underline{\mathbf{D}} = \underline{\varepsilon}\,\underline{\mathbf{E}}, \tag{11}$$

where $\underline{\varepsilon} = \underline{\varepsilon}_\mathrm{r}\varepsilon_0$ is the complex absolute permittivity and $\underline{\varepsilon}_\mathrm{r}$ is the complex relative permittivity.

The complex relative permittivity can be written as:

$$\underline{\varepsilon}_\mathrm{r} = |\underline{\varepsilon}_\mathrm{r}|\,\mathrm{e}^{-\mathrm{j}\delta} = \varepsilon_\mathrm{r}' - \mathrm{j}\,\varepsilon_\mathrm{r}'' = \varepsilon_\mathrm{r}'(1 - \mathrm{j}\tan\delta), \tag{12}$$

where $|\underline{\varepsilon}_\mathrm{r}|$ is the modulus, $-\delta$ is the argument, ε_r' is the real part, $-\varepsilon_\mathrm{r}''$ is the imaginary part, and $\tan\delta = \varepsilon_\mathrm{r}''/\varepsilon_\mathrm{r}'$ is the loss tangent. The minus sign is introduced because the vector **D** lags behind **E**; the argument of $\underline{\varepsilon}_\mathrm{r}$ is negative, but $\delta > 0$. Obviously, $-\delta$ is the phase difference between **D** and **E**. Further, $|\underline{\mathbf{D}}| = |\underline{\varepsilon}_\mathrm{r}|\,\varepsilon_0\,|\underline{\mathbf{E}}|$ so that $|\underline{\varepsilon}_\mathrm{r}|$ plays a role similar to ε_r in a static field.

Since $\mathbf{D}(t)$ and $\mathbf{E}(t)$ are collinear, we can introduce an axis collinear with these two vectors and consider the projections $D(t)$ and $E(t)$ on this axis. These projections are time-harmonic quantities. We consider the plot shown in Fig. 6, where the abscissa is $E(t)$ and the ordinate is $D(t)$. If $D(t)$ and $E(t)$ are in phase, the point in this plane periodically moves along a straight line (the red dashed line in Fig. 6). If they are not in phase, the point moves along an

ellipse in the counter-clockwise direction, creating a hysteresis loop (Rayleigh loop). Such a loop indicates that the dielectric is lossy. The volume density of the energy loss during one cycle is proportional to the surface area bounded by the ellipse, i.e.,

$$\frac{\mathrm{d}w_\mathrm{h}}{\mathrm{d}v} = \varepsilon_\mathrm{r}''\varepsilon_0 |\underline{\mathbf{E}}|^2 = \varepsilon_\mathrm{r}'\varepsilon_0 |\underline{\mathbf{E}}|^2 \tan\delta, \qquad (13)$$

where $|\underline{\mathbf{E}}|$ is the rms of the electric field. Obviously, the larger is $\tan\delta$, the larger are the losses. Hence, $\tan\delta$ is referred to as the dissipation factor.

Note that in our model $-\varepsilon_\mathrm{r}''$ describes all losses in the dielectric: both polarization and ohmic. If needed, the losses may be described by the equivalent conductivity of the medium (σ) and $-\mathrm{j}\varepsilon_\mathrm{r}''$ replaced in (12) by $-\mathrm{j}\dfrac{\sigma}{\omega\varepsilon_0}$.

For high-quality (low-loss) dielectrics, δ is small, $\tan\delta \ll 1$, and $\varepsilon_\mathrm{r}' \approx |\underline{\varepsilon}_\mathrm{r}|$. What can be considered as a low-loss dielectric, depends on applications. For example, in microwave engineering, for frequencies about 1 GHz, $\tan\delta$ of the order of 0.001 can usually considered to be low.

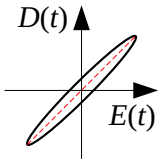

Fig. 6. Hysteresis loop.

The real and the imaginary parts of the complex permittivity are functions of frequency. Due to the causality conditions [41], these functions must satisfy the Hilbert transform (or, equivalently, the Kramers-Kronig relations). Hence, under certain conditions and limitations, if we know ε_r', we can reconstruct $-\varepsilon_\mathrm{r}''$, and vice versa. An important consequence of these relations is that if ε_r' changes with frequency, $-\varepsilon_\mathrm{r}''$ must be nonzero, or, practically speaking, the material must be lossy.

If we need to extract the function $\underline{\varepsilon}_\mathrm{r}(f)$ from measured data, it is convenient to approximate it by an analytic function of the complex frequency $\underline{s}$ ($\underline{s} = \mathrm{j}\omega$ on the imaginary axis of the complex plane), as done, for example, in [42] for FR-4, a material that has an almost constant loss tangent in a very broad frequency range.

IV. Measurement Techniques

Various methods and equipment can be used for measurement of the dielectric parameters [43], depending on the frequency range, aggregate state of samples, shape and size of available samples, etc.

For lower frequencies, up to about 100 MHz, the most commonly used method is based on inserting the material sample between two parallel electrodes, thus forming a parallel-plate capacitor. The capacitance is measured and the dielectric parameters are identified from the result. This technique is simple and convenient for solid samples in many cases. However, for barium titanate, magnesium titanate, and similar high-permittivity materials, air gaps between the sample and the electrodes are formed, which reduce the accuracy. Also, the measurement structure cannot be assumed to be quasistatic already at about 100 MHz. At higher frequencies, internal resonances may occur and jeopardize the measurements.

As the frequency increases, the parallel-plate capacitor has a strong electromagnetic coupling with the environment and it must be shielded. However, the shield creates a resonant cavity, which further aggravates the measurements. In order to push these resonances towards higher frequencies, the size of the cavity should be small.

Another problem with the parallel-plate structure is that it requires samples of an appropriate shape and size. For example, commercially available meters (such as Agilent E4991A meter with Agilent 16451B probe) require a large sample diameter (at least 15 mm), whereas our samples of ceramic materials are much smaller (often up to around 8 mm in diameter). Examples are pill-shaped sintered samples [44], which practically cannot be machined or otherwise adapted to the measurement system.

The parallel-plate capacitor measurement technique is convenient for liquid dielectrics. The main limitation is the relatively low upper frequency limit.

For frequencies above about 1 GHz, open coaxial lines can be used to characterize various materials [45]. This method is convenient because it usually does not require special forming of the sample. However, in order to provide accurate measurements, the sample should be big enough and it tightly positioned on the coaxial-line opening.

It is also possible to characterize a material by placing a sample between two antennas and measure the transfer between the antennas [46]. However, relatively large samples are required (e.g., in the form of a large sheet). Similar techniques exist for measurements in coaxial and waveguide systems [47], but they usually require that the samples have an appropriate shape and dimensions.

Dielectric substrates used in microwave engineering can be characterized by various resonant methods [48]. However, these are narrowband techniques. In order to provide data for a wide frequency band, other techniques can be used, such as manufacturing and measuring various transmission lines [42], which also require a special shape of the dielectric or metallization.

In [49], a method is described that was designed specifically for measurements of samples of ceramic materials that have a cylindrical shape (i.e., a pill-shape) and whose dimensions correspond to the majority of our samples. We have developed a small coaxial chamber, which is, naturally, shielded from the environment. We measure the reflection coefficient of the chamber using a network analyzer and then apply numerical techniques to extract the complex relative permittivity of the sample. However, this chamber requires that the bases of the cylinder are metallized. This can be done using silver-based conductive ink, which does not adhere well to ceramic materials and is messy for application.

We have further improved the measurement method by machining a new coaxial chamber (Fig. 7) and developing the corresponding software for measurements at frequencies in the VHF band [50]. In the meantime, we have developed

new numerical models that enable us to perform measurements up to around 10 GHz. We briefly describe this method in the following paragraphs.

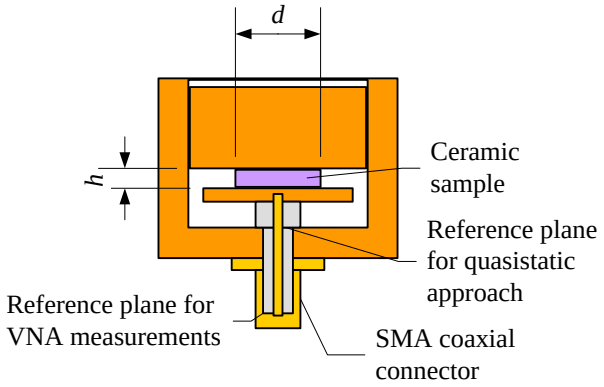

Fig. 7. Sketch of the test fixture for measurement of dielectric parameters of sintered samples.

The test fixture is a rotationally-symmetrical structure. It comprises a standard SMA coaxial connector at the bottom. The inner conductor of the connector carries a thin metallic disc, which acts as the lower electrode of a parallel-plate capacitor. The upper electrode is a thick metallic disc, which has a screw thread whose pitch is 1 mm. A mating thread is cut in the outer wall of the chamber. The upper electrode can be removed from the chamber so that a ceramic sample can be inserted into the chamber. The upper electrode is placed back so that it lightly presses the sample.

The ceramic sample is cylindrical, its diameter is *d*, and the height is *h*.

All metallic parts of the chamber are made of brass, except for the coaxial SMA connector, which is made of gold-plated stainless steel. The dielectric of the connector is Teflon. A Teflon disk is placed under the lower electrode in order to restrict the pressure on the inner conductor of the SMA connector.

We use a vector network analyzer (VNA) Agilent E5061A to measure the reflection coefficient at the SMA connector. The VNA is calibrated using an SMA calibration kit. The reference plane is at the lower end of the SMA connector.

At lower frequencies, up to around several hundred MHz, the chamber is assumed to be small compared to the wavelength and the quasistatic approximation for the electromagnetic fields is applied. The chamber is numerically modeled using a similar approach as in [51, 52]. A set of integral equations for the total charges (free plus bound) is formulated based on the boundary conditions. The first subset of boundary conditions is for the potential at conductor surfaces. The second subset of boundary conditions is for the normal component of the electric field at dielectric-to-dielectric interfaces. This system of integral equations is solved using the method of moments [53] with a piecewise-constant approximation for the charge distribution. The Galerkin technique is applied for testing.

The integrals for the potential are double. The first integration is carried out analytically, using the complete elliptic integral of the first kind. For the second integration, an adaptive Gauss-Legendre formula. The Galerkin integration is implemented using a Gauss-Legendre formula applied to equal-length subsegments along the generatrix of the structure.

The normal component of the electric field is obtained by numerical differentiation of the potential. Thereby, the field segment is incrementally moved away, perpendicularly from its original position, and the potential is evaluated for two positions of this segment.

In the numerical model, the conductors are assumed to have a finite thickness. Hence, the surface density of the free charges on the conductors is extracted from the density of the total charges by multiplication by the relative permittivity of the surrounding dielectric. In comparison with the method used in [51, 52], this approach significantly improves the quality of the solution.

The dielectric losses of the ceramic sample are taken into account by using the complex relative permittivity. The complex capacitance of the chamber is extracted from the measured complex admittance and the complex permittivity of the sample is adjusted in the numerical model so that the computed capacitance matches the measured one. This adjustment involves several interpolations.

For smaller ceramic samples, a simpler procedure is possible. The complex capacitance is measured when the sample is present and when it is removed. The complex relative permittivity of the sample is thereafter evaluated from the difference of these two capacitances, assuming that the electric field within the sample is homogeneous.

The accuracy of the quasistatic approach is enhanced by shifting the VNA reference plane to the beginning of the chamber (Fig. 7). Additionally, a first-order correction is implemented for the parasitic inductance of the chamber. As the result, the measurements can be performed in the whole VHF frequency band (30–300 MHz) and even extended to 500 MHz. The measurement uncertainty is 2% for ε_r' and 0.003 for $\tan\delta$. At lower frequencies, the VNA noise becomes a problem, which jeopardizes measurements particularly below around 10 MHz.

For higher frequencies, we have developed full-wave models of the chamber in software WIPL-D [54] and HFSS [55]. The models include the feeding coaxial line, up to the reference plane for VNA measurements. In each model, we supply the geometrical dimensions of the chamber and the sample, as well as data for the conductors (brass, gold) and dielectrics (Teflon, air) of the chamber. We assume several values for the relative permittivity of the sample and sweep over the frequency to compute the reflection coefficient at the reference plane for VNA measurements. Finally, we interpolate the relative permittivity to obtain the best agreement with the measurements.

V. Examples of Measured Permittivities

We present two examples in order to illustrate how the dielectric parameters of ceramic materials are affected by the mechanical activation (Section II) and also demonstrate the results obtained by the measurement technique described in Section IV.

The first example is spinel ceramic ($MgAl_2O_4$) [56]. We examined two different powders. One was not activated and the other one was activated in a high-energy planetary ball mill for 60 min. The results of the particle-size analysis (PSA) are shown in Fig. 8. The average particle size d(0.5)

was 2.1 µm for the non-activated powder AM–0. After mechanical activation for 60 minutes, the average particle size decreased to about 1.3 µm. Likewise, d(0.1) decreased from 0.69 µm for AM–0 to 0.43 µm for AM–60. Interestingly, d(0.9) increased from 4.74 µm for AM–0 to 8.04 µm for AM–60. Milling also produced a bimodal particle-size distribution in the AM–60 powder with peaks in the distribution at about 0.8 µm and 5 µm. While the milling significantly reduced the average particle size, it also produced some agglomerates that were larger than in the starting powder.

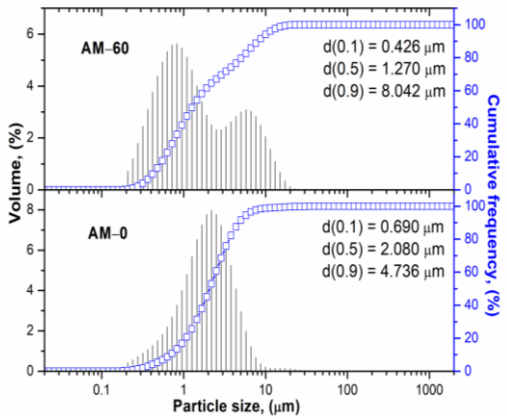

Fig. 8. PSA of the non-activated powder (AM–0) and powder activated for 60 minutes (AM–60).

Fig. 9a shows the relative permittivity and loss tangent of the material, sintered at 1400 ºC for 2h, when the starting powders (MgO and Al_2O_3) were not mechanically activated. These dielectric parameters are shown as a function of frequency in the range from 10 MHz to 500 MHz. The material is lossy; the loss tangent exceeds 0.3 at 10 MHz. The relative permittivity decreases with frequency, which is in accordance with the causality conditions.

Fig. 9b shows the results for spinel, also sintered at 1400 ºC for 2h, when the starting powders were activated. The relative permittivity is increased compared to the non-activated material and the loss tangent is smaller. The increased relative permittivity is in agreement with the increased density: the density of the non-activated material is 2.05 g/cm^3, whereas the density of the activated material is higher, 2.22 g/cm^3.

The second example is cordierite [57], which was mechanically activated. The milling times were up to 160 minutes. Also in this case, a strong correlation was found to exist between ε'_r and the sample density (ρ): the relative permittivity is higher for denser samples (i.e., for samples which have lower porosity), as shown in Fig. 10.

The data points in Fig. 10 closely follow the Lichtenecker-Rother logarithmic law of mixing [58]. The density of cordierite without pores is $\rho = 2.6\,\mathrm{g/cm^3}$, for which this fitting formula yields $\varepsilon'_r = 6.1$.

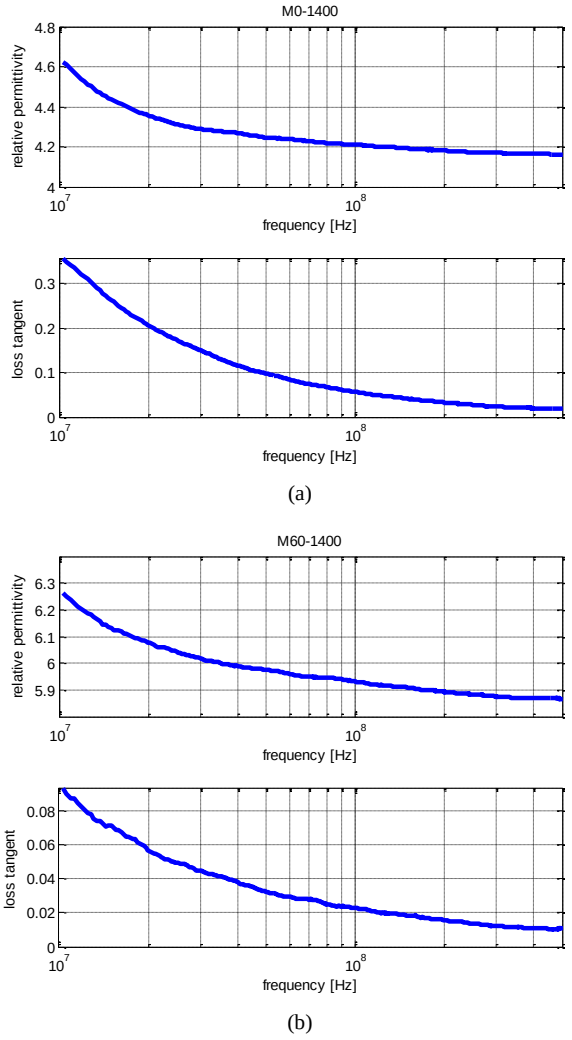

Fig. 9. Relative permittivity and loss tangent, as a function of frequency, for spinel when the starting powders were (a) not activated and (b) activated by milling for 60 minutes.

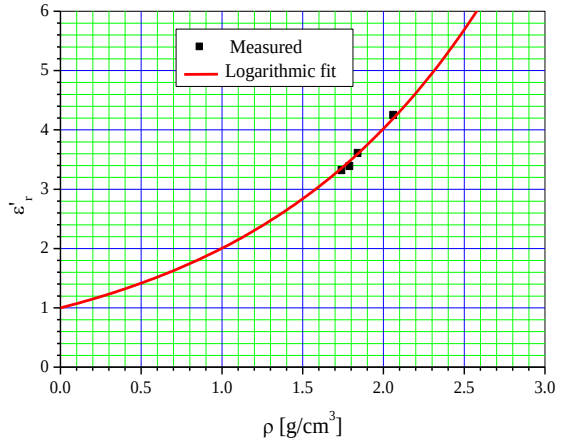

Fig. 10. Real part of the relative complex permittivity versus density for cordierite [57].

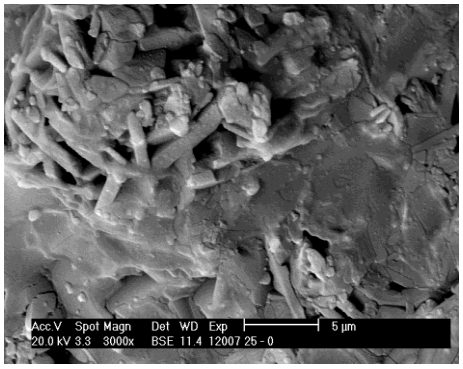

(a)

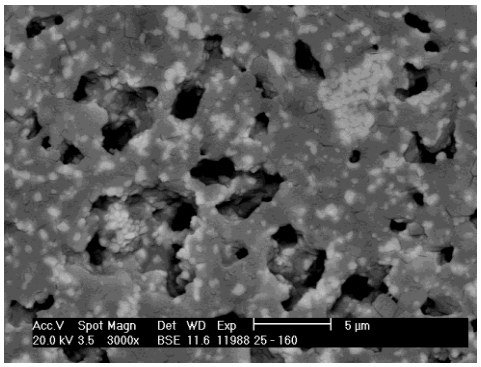

(b)

Fig. 11. SEM micrographs of two-step sintered powder mixtures: (a) MAS-0-S2 and (b) MAS-160-S2.

The average sample densities after the two-step sintering regime ranged from 60.3 to 74.8 % of the theoretical density. The scanning electron micrographs of the two-step regime sintered samples are shown in Fig. 11. The MAS-0-S2 sample (non-activated) consists of two different areas. One is a well sintered matrix and the other one is made of rod-like parts where the sintering process had not finished. This microstructure is a consequence of non-homogeneous mixture sintering. The sample MAS-160-S2 (activated for 160 minutes) has the highest relative density and the lowest relative open porosity. The obtained microstructures and densities after sintering are in a good accordance with the results of electrical measurements.

VI. Conclusions

Preparation conditions influence significantly the final structure and electrical properties of ceramic materials. An important goal is to obtain a ceramic material with nearly the full density and fine grains with a homogeneous distribution. The mechanical activation, as a pretreatment for the shaping and sintering process, is a very convenient way of powder preparation with a uniform particle-size distribution [59]. Processes such as increase in the number of contact and massive neck formation occur during the early stage of sintering. The neck growth is controlled by numerous diffusion mechanisms whose rates are determined by the total flux of atoms coming to the neck, suggesting that the dominant processes occur at grain boundaries.

Many functional properties of ceramics are also strongly influenced by the grain boundaries. From that point of view, electrical properties must be measured using AC techniques, so that the effects of grains and grain boundaries can be assessed separately.

Furthermore, sintering conditions can drastically change electrical properties. We considered the influence of the mechanical activation on the permittivity and the loss tangent of ceramic materials. We presented several examples demonstrating this influence. The results for the permittivity and the loss tangent were obtained using a newly developed measurement technique, which is revealed in the paper. The technique was designed to characterize relatively small samples of ceramic materials, without the need to metallize the surfaces of the samples. The electrical parameters in the VHF frequency band are computed from measured data using a quasi-static model. For higher frequencies, in the microwave region up to 10 GHz, we developed full-wave models, which are yet to be fully verified.

Acknowledgment

This research was performed within Projects OI 172057 and TR 32005 funded by the Ministry of Education, Science and Technological Development of the Republic of Serbia, and within Project F133 funded by the Serbian Academy of Sciences and Arts.

References

[1] http://www.linkinternationalkl.com/did-you-know-the-word-ceramics-comes-from-the-greek/
[2] P. L. Wise et al., Structure microwave property relations of Ca and Sr titanates, J. Eur. Ceram. Soc., 21 (2001) 2689-2632.
[3] С. Я. Гордеев, Физико-хемические основы керамической технологии, ИХТИ, Иваново, 1979.
[4] S. J. L. Kang, Sintering, densification, grain growth & microstructure, Elsevier, 2005.
[5] A. M. Maričić, S. M. Radić, M. M. Ristić, Fizički i fizičkohemijski principi tehnologije keramičkih materijala, Monografije nauke o materijalima, 37 CMS BU, Beograd, 1998.
[6] M. M. Ristić, S. Đ. Milošević, Mechanical activation of inorganic materials, SASA Monographs 38, Beograd, 1998.
[7] Е. Г. Аввакумов, Механические методы активации хумических процессоб, Новосибирск: Изд-во Наука, Сибирское отд-ние, 1986.
[8] Lj. D. Andrić, Mehanohemijska aktivacija glinice i njen uticaj na promenu kristalne strukture, doktorska disertacija, BU, Beograd, 1999.
[9] A. Branković et al., Mechanochemical Activation of (SeO_2+Na_2CO_3) Mixture and Sodium Selenite Synthesis in Vibrational Mill, J. Sol. St. Chem., 135 (1998) 256–259.
[10] N. Obradović, Uticaj aditiva na sinterovanje sistema ZnO-TiO_2 saglasno trijadi "sinteza-struktura-svojstva", doktorska disertacija, BU, Beograd, 2007.
[11] А. С. Баланкин, Самоорганизация и диссипативные структуры в деформируемом теле, Письма в Журнал Технической Физики, 16 (1990) 14–20.
[12] G. Heinicke, Tribochemistry, Academie-Verlag, Berlin, 1984.
[13] П. Ю. Бутягин, Кинетика и природа механохемических реакций, Успехи хемии, 40 (1971) 1935–1959.
[14] S. Filipović, Uticaj mehaničke aktivacije na svojstva MgO-TiO_2 elektrokeramike, doktorska disertacija, Tehnički fakultet u Čačku, Univerzitet u Kragujevcu, 2014.
[15] M. M. Ristić, Principi nauke o materijalima, Posebno izdanje knjiga DCXVII, SANU, Beograd, 1993.
[16] E. Kostić et al., Activation of solid state processes in Sintering and Materials, International Academic Publishers, Beijing, (1995) 142–147.
[17] N. Đorđević, N. Obradović, D. Kosanović, M. Mitrić, V. B. Pavlović, Sintering of Cordierite in the Presence of MoO_3 and Crystallization Analysis, Sci. Sinter., 46 (2014) 307–313.
[18] A. Peleš, V. P. Pavlović, S. Filipović, N. Obradović, L. Mančić, J. Krstić, M. Mitrić, B. Vlahović, G. Rašić, D. Kosanović, V. B. Pavlović, Structural investigation of mechanically activated ZnO powder, J. Alloys and Comp., 648 (2015) 971–979.
[19] N. Obradović, N. Labus, T. Srećković, S. Stevanović, Reaction Sintering of the 2ZnO-TiO_2 System, Sci. Sinter., 39 (2007) 127–132.

[20] G. Chen et al., Effects of mechanical activation on structural and microwave absorbing characteristics of high titanium slag, Powd. Technol., 286 (2015) 218–222.
[21] B. S. Zlatkov, M. V. Nikolić, V. Zeljković, N. Obradović, V. B. Pavlović, O. Aleksić, Analysis and modeling of sintering of Sr-hexaferrite produced by PIM technology, Sci. Sinter., 43 (2011) 9–20.
[22] T. Tunç, A. Ş. Demirkıran, The effects of mechanical activation on the sintering and microstructural properties of cordierite produced from natural zeolite, Powd. Technol., 260 (2014) 7–14.
[23] D. Kosanović, J. Živojinović, N. Obradović, V. P. Pavlović, V. B. Pavlović, A. Peleš, M. M. Ristić, The influence of mechanical activation on the electrical properties of $Ba_{0.77}Sr_{0.23}TiO_3$ ceramics, Ceram. Inter., 40 (2014) 11883–11888.
[24] S. Filipović, N. Obradović, V. Petrović, Influence of Mechanical Activation on Structural and Electrical Properties of Sintered $MgTiO_3$ Ceramics, Sci. Sinter., 41 (2009) 117–123.
[25] N. Obradović, N. Mitrović, V. Pavlović, Structural and electrical properties of sintered zinc-titanate ceramics, Ceram. Inter., 35 (2009) 35–37.
[26] M. M. Ristić, N. Obradović, S. Filipović, A. Bykov, M. A. Vasilkovskaya, L. A. Klochkov, I. I. Timofeeva, Formation of magnesium titanates, Powd. Metall. Metal. Ceram., 48 (2009) 371–374.
[27] A. N. Maratkanova et al., Structural characterization and microwave properties of chemically functionalized iron particles obtained by high-energy ball milling in paraffin-containing organic environment, Powd. Technol. 274 (2015) 349–361.
[28] N. Obradović, S. Filipović, N. Đorđević, D. Kosanović, S. Marković, V. Pavlović, D. Olćan, A. Đorđević, M. Kachlik, K. Maca, Effects of mechanical activation and two-step sintering on the structure and electrical properties of cordierite-based ceramics, Ceram. Inter., 42 (2016) 13909–13918.
[29] M. V. Nikolić, N. Obradović, K. M. Paraskevopoulos, T. T. Zorba, S. M. Savić, M. M. Ristić, Far infrared reflectance of sintered Zn_2TiO_4, J. Mater. Sci., 43 (2008) 5564–5568.
[30] H. B. Jin et al., Influence of mechanical activation on combustion synthesis of fine silicon carbide (SiC) powder, Powd. Technol., 196 (2009) 229–232.
[31] Г. В. Самсонов, Конфигурационние представления електроного строения в физическом материаловедении, Наукова Думка, Киев, 1977.
[32] https://www.google.com/search?q=three+stages+of+sintering&client=firefox-b-d&source=lnms&tbm=isch&sa=X&ved=0ahUKEwjzouiAvbjhAhVBaVAKHbf5DJoQ_AUIDigB&biw=1366&bih=654#imgrc=sIJp7eWFmCmlwM:
[33] Ya. I. Frenkel, Viscous flow of crystalline bodies under action of surface tension, J. Phys., 9 (1945) 385.
[34] V. V. Srdić, Presovanje novih keramičkih materijala, Tehnološki fakultet, Novi Sad, 2004.
[35] R. M. German, Sintering-Theory and Practice, John Wilez & Sons, Inc., New York, 1996.
[36] M. N. Rahaman, Ceramic processing and sintering, Marcel Dekker, Inc. New York, 2003.
[37] L. C. De Jonghe, M. N. Rahaman, Sintering of ceramics, Handbook of applied ceramics, Elsevier, 2003.
[38] A. R. Djordjević, Fundamentals of Electrical Engineering, Part IV, AC Currents, Belgrade: Academic Mind, 2016.
[39] A. R. Djordjević, Electromagnetics, Belgrade: Academic Mind, 2008.
[40] A .R. Djordjević, Fundamentals of Electrical Engineering, Part I, Electrostatics, Belgrade: Academic Mind, 2016.
[41] A. R. Đorđević, D. V. Tošić, "Causality of circuit and electromagnetic-field models", Proc. of 5th European Conference on Circuits and Systems for Communications (ECCSC'10), pp. 12–21, Belgrade, Serbia, 2010.
[42] A. R. Djordjević, R. M. Biljić, V. D. Likar-Smiljanić, T. K. Sarkar, "Wideband Frequency-Domain Characterization of FR-4 and Time-Domain Causality", IEEE Trans. Electromagn. Compat., vol. 43, no. 4, pp. 662–667, 2001.
[43] O. V. Tereshchenko ; F. J. K. Buesink ; F. B. J. Leferink, "An overview of the techniques for measuring the dielectric properties of materials", General Assembly and Scientific Symposium, vol. 1320, pp. 1–4, Istanbul, Turkey, 2011.
[44] N. Obradovic, M. V. Nikolic, N. Nikolic, S. Filipovic, M. Mitric, V. Pavlovic, P. M. Nikolic, A. R. Đordevic, M. M. Ristic, "Synthesis of barium-zinc-titanate ceramics", Science of Sintering, vol. 44, no. 1, pp. 65–71, 2012.
[45] T. P. Marsland, S. Evans, "Dielectric Measurements with an Open-ended Coaxial Probe", IEE Proc. Microw., Antennas Propag., vol. 134, pp. 341–349, 1987.
[46] D. K. Ghodgaonkar, V. V. Varadan, "A Free-space Method for Measurement of Dielectric Constants and Loss Tangents at Microwave Frequencies", IEEE Trans. Instrum. Meas., vol. 37, no. 3, pp. 789–793, 1989.
[47] A. M. Nicolson, G. F. Ross, "Measurement of the Intrinsic Properties of Materials by Time Domain Techniques", IEEE Trans. Instrum. Meas., vol. IM–19, no. 4, pp. 377–382, 1970.
[48] http://literature.cdn.keysight.com/litweb/pdf/5989-5384EN.pdf
[49] A. Djordjević, J. Dinkić, M. Stevanović, D. Olćan, S. Filipović, and N. Obradović, "Measurement of permittivity of solid and liquid dielectrics in coaxial chambers", Microwave Review, Vol. 22, No. 2, December 2016, pp. 3–9.
[50] A. Đorđević et al., Chamber for Measurement of Relative Permittivity and Loss Tangent of Dielectrics, School of Electrical Engineering, University of Belgrade, Project TR32005, 2018.
[51] A. R. Djordjević, M. B. Baždar, R. F. Harrington, and T. K. Sarkar, LINPAR for Windows: Matrix Parameters for Multiconductor Transmission Lines, Artech House, Norwood, MA, 1999.
[52] M. M. Nikolić, A. R. Djordjević, and M. M. Nikolić, ES3D: Electrostatic Field Solver for Multilayer Circuits, Artech House, Norwood, MA, 2007.
[53] R. F. Harrington, Field Computation by Moment Methods, Wiley-IEEE Press, Hoboken, NJ, 1993.
[54] WIPL-D. Wipl-d pro 11.0. WIPL-D, 2013, http://www.wipld.com
[55] ANSYS. Ansys hfss 15.0.0. ANSYS, 2014, http://www.ansys.com
[56] N. Obradović, W. G. Fahrenholtz, S. Filipović, D. Kosanović, A. Dapčević, A. Đorđević, I. Balać, V. Pavlović, "The effect of mechanical activation on synthesis and properties of $MgAl_2O_4$ ceramics", Ceramics International 45 (2019) 12015–12021.
[57] N. Obradović, Synthesis of Cordierite-Based Ceramics, Belgrade: Academic Mind, 2016.
[58] K. Lichtenecker and K. Rother, Die Herleitung des logarithmischen Mischungsgesetz es aus allgemeinen Prinzipien der stationären Strömung: Physikalische Zeitschrift, 32 (1931) 255–260.
[59] S. Filipović, V. P. Pavlović, N. Obradović, V. Paunović, K. Maca, V. B. Pavlović, "The impedance analysis of sintered $MgTiO_3$ ceramics" Journal of Alloys and Compounds 701 (2017) 107–115.